**Agencywide Document Access and Management (ADAMS),
ML20118C424, U.S. Nuclear Regulatory Commission (NRC), October 2018**

Long-Term Initiation Time for Stress -Corrosion Cracking of Alloy 600 and Stainless Steel: Review and Analysis for Nuclear Application

Tae M. Ahn
Office of Nuclear Material Safety and Safeguards
U.S. Nuclear Regulatory Commission
Washington, DC 20555-0001, USA

Abstract

This paper provides a summary and analysis on the initiation of stress -corrosion cracking (SCC) of Alloy 600 (and related alloys) and stainless steels in nuclear reactor environments near 300 ˚C. Two processes seem to be comparable between traditional slip dissolution/oxidation mechanisms and aging--related crystalline ordering. This paper evaluates various supporting topics, including SCC initiation time, activation energy, stress/strain rate/plastic deformation, electrode potential drop, rate--limiting step, long--term threshold values, and data uncertainties. The understanding of Alloy 600 SCC is extended to stainless steels. SCC mechanisms of nickel--based alloys and stainless steels are different from nickel-l--based alloys at lower temperatures. Finally, this paper describes how this work would be potentially considered in the nuclear industry.

Disclaimer

The U.S. Nuclear Regulatory Commission (NRC) staff views expressed in this paper are preliminary and do not constitute a final judgment or determination of the matters addressed or the acceptability of any licensing action the NRC may be considering.

Corresponding author: tae.ahn@nrc.gov. (tel) +1 301 415 5972

Key Words: Stress-Corrosion Cracking, Crystalline Ordering, Alloy 600, Stainless Steel, Initiation, Review and Analysis

1. Introduction

Nuclear reactors have components made of Alloy 600, a nickel--based alloy. Stress-corrosion cracking (SCC) has been observed over the past 20 years of reactor operations. Although the propagation of SCC has been studied extensively, the long initiation time of SCC has had very little attention. The material aging has long been studied, and crystalline disorder--to--order state has been studied more recently. Recently, more attention has been directed to the effect of crystalline ordering (i.e., ordering, unless otherwise specified) on reactor SCC.

With more traditional experience in Alloy 600, this paper presents a literature review and analysis of several topics. With the crystalline ordering concept, this paper reconsiders relevant traditional SCC mechanisms and data on Alloy 600 in nuclear reactor environments at, above, or near 300 ˚C. It also includes related data on nickel-based alloys as appropriate because the general SCC properties do not change substantially. In the analysis, important topics covered include traditional SCC mechanisms, the crystalline ordering process, crack initiation time, activation energy, stress/strain rate/plastic deformation, electrode potential drop, rate--limiting steps, data uncertainties, - low temperature SCC, and long--term threshold values for SCC initiation. Based on this review and analysis, this paper also discusses lower temperature SCC (near 100 ˚C). On this basic frame of understanding, the present consideration is applied to stainless steel. A separate section looks at some stainless steels used for nuclear applications. Finally, this paper describes how the information is applied across the nuclear industry.

2. Data on SCC Initiation Times of Alloy 600 (or Related Nickel--Based Alloys) in the Literature and Nuclear Reactor Operations

The table below summarizes relevant data that are discussed in this paper. The data include results from laboratory tests, nuclear reactor operational experiences, and interpretations of all information for safe reactor operations. All data were obtained in water, except for the creep test, which were obtained in air (Arioka, 2015). The data focus on the following:

- source
- alloy type
- environment
- SCC test temperature (˚C)
- SCC initiation time (year)
- activation energy (kilojoules per mole (kJ/mol))
- preaging for crystalline ordering transformation
- stress present
- remarks

The section below provides detailed data interpretation and discussion.

Summary of Literature and Reactor Data on SCC Initiation Time in Nickel-Based Alloys (mainly Alloy 600)

Author	Content
Scott (2018)	Alloy 600; reactor environment; 280 to 320 ˚C—17 to 27 reactor years, minimum failure time of 0.7 to 10.4 years (minimum 1.14 years at 325 degree C and 450 megapascals (MPa)), reactor, varying temperature and stress, no preaging; 308 kJ/mol, example cases
Moss et al. (2018)	Nickel-33 chromium; reactor water; 313 ˚C—0.033 year; 33 MPa $m^{1/2}$; preaging at 475 ˚C—0.02 year (ordering initiation, continued to grow ordering)
Yoo et al. (2018)	Alloy 600; reactor water; 315 and 340 ˚C—0.02 to 0.06 years, preaging 400 ˚C—0.13, 0.26 years (ordering propagation); as-received, 0.04, 0.06 years; slow strain rate test
Andresen and Chou (2018)	Alloy 600; deaerated and demineralized, and hydrogenated water; 360 ˚C, 0.004 to 0.13 years, 325 ˚C, 0.04 year; no preaging; constant load (greater than yield stress)
Zhai et al. (2015)	Alloy 600 (690); reactor primary water; 360 ˚C—0.14 to 0.85 year (cold work/stress dependence); no preordering
Arioka (2015)	Alloy 690; reactor primary water, air; 360 to 465 ˚C; 450 ˚C—0.34 years (air), 360 ˚C—3.0 years (water), 1.9 years (air), 320 ˚C—3.4 years (water); no preaging; the only air data included
Scott (2013)	Alloy 600; reactor environment, 6 to 11.4 years, no preaging; operating experience
Yonezawa (2013)	Alloy 600; reactor water; 332 ˚C—1.3 to 1.9 years; no preaging; round robin test
Richey and Morton (2005)	Alloy 600; high -purity water with hydrogen; 360 ˚C—0.23 year; no preaging; 550 MPa
Grimmel and Cullen (2005) NRC	Alloy 600; reactor water; 275 to 315 ˚C—11 to 24 years; no preaging; reactor operational experience
Casagne et al. (1992)	Alloy 600; deaerated with hydrogen; 316 ˚C—0.77 years, 288 ˚C—7.7 years; 212 kJ/mol; no preaging; U-bend –U-bend and C-ring (385 to 840 MPa)
Economy et al. (1987)	Alloy 600; demineralized and hydrogen-containing water; 333 ˚C—2.5 years; 179 kJ/mol; no preaging; U--bend
Garud and McIlree (1986)	Alloy 600; high -purity water; 350 ˚C—0.114 to 1.14 years, 290 ˚C—0.228 to 11.4 years; no preaging; 210 to 525 MPa; model

3. Interpretation and Analysis

Alloy 600 has a typical composition of 72 nickel (Ni)–(14–17) chromium (Cr)–(6–10) iron (Fe) (in weight %) and is fabricated by mill-annealing, is plastically deformed, or both. The nuclear reactor components made of Alloy 600 include steam generator tube, instrument nozzle, and heater thermal sleeves. Other new alloys, such as Alloy 690, are also being used. The service environments are mainly deaerated/demineralized water, typically with an oxygen level less than 10 parts per billion (ppb) and often hydrogenated with hydrogen gas. The temperature ranges around 300 ˚C, often higher for accelerated tests, to simulate longer time service at a lower temperature. SCC initiation time is the primary focus of this paper.

3.1 Important Stress-Corrosion Cracking Mechanisms

Slip dissolution (Ford and Andresen, 1988; Andresen and Ford, 1985) and oxidation (Shen et al., 2018; Capell and Was, 2007; Scott and Le Calvar, 1993) are two commonly known SCC mechanisms and models. These two models are interchangeable. Other mechanisms and models include electrochemical potential (Staehle, 2001), creep (Arioka, 2015; Yi et al., 2013; Angeliu et al.,1995) at temperatures above 350 ˚C, and electrochemistry (Lee and Macdonald, 2018). In the slip dissolution model, passive film forms with a very low -dissolution rate and film ruptures by strain to exposed bare metal surface for fast dissolution.

Normally, strain rates are compared with a repassivation rate. If strain rates (in log scale) are faster compared with repassivation rates (in log scale), mechanical failure occurs. If strain rates are slower, metals will dissolve very slowly by passivation. Additionally, strain rates in a certain range may harmonize with dislocation (or other defect) dynamics for crack propagation once the crack is initiated. Therefore, under optimum ranges of strain rates, SCC would occur (Jones, 1992; Ugiansky and Payer, 1979). Under static stress conditions, stress above yield stress is normally regarded as dynamic (like strain rate) because of dislocation mobility, which may promote SCC. It is noted that the yield stress decreases at elevated temperature.

The oxidation model is based on oxide formation, especially in grain boundaries, being subjective to cracking. The creep model would occur at grain boundaries by cavity formation induced by point defect mobility. The electrochemistry model is based on the localized electrochemistry. It is noted that many data showed intergranular stress-corrosion cracking (IGSCC). However, there were exceptions that showed IGSCC occurred beneath to crack surface dimple cracks (Kim et al., 2015; Angeliu et al., 1995). This is considered to be caused by high stress applied on the crack surface, which then forms dimple cracks and IGSCC at lower stress below the cracked surface.

3.2 Crystalline Ordering Process

Very recently, the crystalline ordering process at high temperatures from a disordered state at ambient temperature has been considered a factor in influencing Alloy 600 SCC (Moss et al., 2018; Kim et al., 2015). The ordered phase is more brittle and harder compared with the disordered phase. Although the NRC identified and evaluated disorder-to--order phase transformation years ago (Dunn et al., 2004), direct consequence is recently being addressed. Some ordering kinetics of nickel-based alloys have been reported (Jackson et al., 2018), but detailed understanding of SCC is very limited. In this regard, the author of this paper recently proposed initiation kinetics of the ordering process in an NRC report, “Nucleation Kinetics of

Crystalline Ordering in Alloy 600 at Elevated Temperature" (Ahn, 2018), which is supported by NRC peer review. A short summary of the work is presented below. The presentation in this paper is an initial attempt to connect the ordering process with other SCC mechanisms.

Fig. 1 presents numerical exercise results of the model of time--temperature--transformation (nucleation or initiation) for the ordering process in Alloy 600. The measured activation energy was 190 kJ/mol from differential scanning calorimetry (Kim et al., 2000). A schematic accompanies the Fig. 2 to compare with the traditional Arrhenius type. The NRC report (Ahn, 2018) contains the details of the numerical values from the calculation. The model results are in agreement with two existing databases (Stephen et al., 2018; Young et al., 2013) and a computer code exercise based on different chemistry representations (Young et al., 2013).

Nucleation time is written with respect to a measured reference time (Ahn, 2018) as follows:

$$\Delta G^{*} \times \exp\left(\Delta G^{*}/[RT]\right) \times \exp\left(E_m/[RT]\right) \qquad \text{(Eq. 1)}$$

where:

ΔG^{*} is activation energy for nuclei population and is a function of temperature (Ahn, 2018).
E_m is activation energy for atomic diffusion for transformation.

Section 3.9 of this paper discusses more details. The nucleation time is proportional to the exponent of activation energy. This means that the sensitivity is very high.

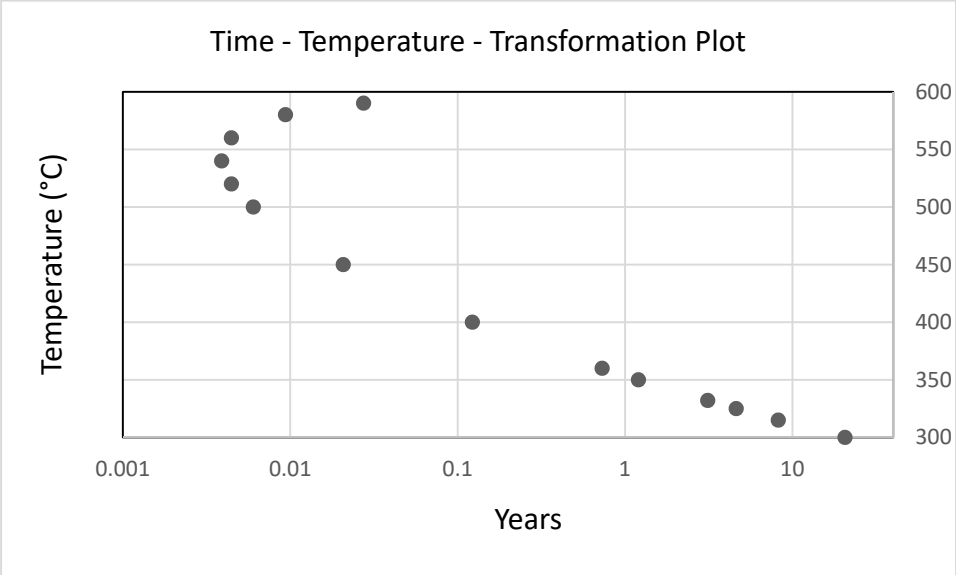

Fig. 1. Time--temperature--transformation C-like curve from Eq. 1 for Alloy 600 (Source: Ahn, 2018).

˚C	590	580	560	540	520	500	450	400	360	350	332	325	315	300
years	0.027	0.009	0.004	0.004	0.004	0.006	0.021	0.123	0.731	1.205	3.128	4.626	8.258	20.651

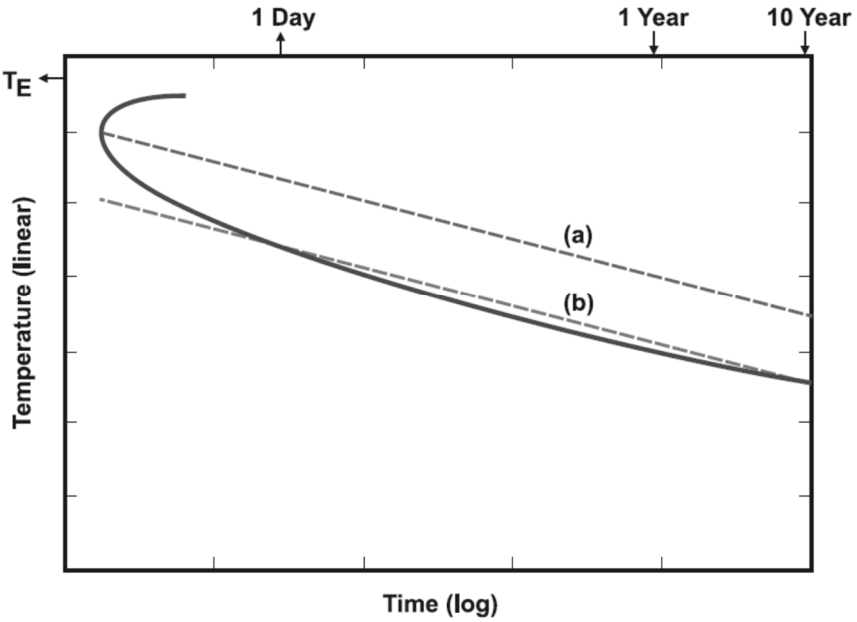

Fig. 2. Traditional linear Arrhenius plot, (a) and (b) for Alloy 600. Actual numerical values given near linear plot. The nucleation times (a) and (b) can be larger or shorter than the curve (as in Fig. 1), which can be an overestimate or underestimate. Also, the nose of the C--like curve is not represented.

3.3 Crack Initiation Time

The purpose of Fig. 1 is to compare the calculated times for nucleation of ordering with the SCC data bases listed above. The data above are selected at the very beginning of SCC to be comparable with the numerical model exercise results (i.e., nucleation) in Fig. 1. Compared with the calculated ordering nucleation time above, the observed SCC data above are mostly the same or shorter in the uncertainty range. However, there are three exceptions of longer times than the calculated nucleation times. The first exception is pre-ordering treatment and SCC testing in water (Moss et al., 2018). The SCC initiation time was much shorter than ordering time, and SCC did not occur without pre-aging. The second is creep data (Arioka, 2015) at higher temperatures. The time for SCC cracking is also longer. It is noted that cracking occurred in air under applied stress. The third exception (Yoo et al., 2018) is SCC data, including prolonged aging (longer time including growth in addition to the order nucleation). The times for the aged sample showed only a slightly shorter time than the unaged sample. Most of the data above have tests from no prior aging (ordering), except two with prior aging (Moss et al., 2018; Yoo et al., 2018). Also, all tests were done in water, except the creep test, which was in air (Arioka, 2015).

Therefore, the implications of this correlation are that both slip dissolution (or oxidation) and ordering could be involved in the SCC initiation. Further, they could occur simultaneously or sequentially. Other sections of this paper present more considerations.

3.4 Activation Energy

Léonard (2010) summarized activation energy for SCC initiation of Alloy 600 in the range of 165–230 kJ/mol. In a more recent review, especially in reactor, the value could be higher (Scott, 2018). Similarly, the activation energies for the ordering process of Ni-Cr-Fe alloys are reported to be 135–275 kJ/mol (more likely, 135–205 kJ/mol) (Young et al., 2013) and 144–225 kJ/mol (Dunn et al., 2004). Both activation energies vary depending on variations in alloy chemistry and crystalline defects (e.g., point defects), secondary phase formation (e.g., carbide), or the fabrication process (e.g., temperature, time, and stress). All these variations sensitively affect the nucleation time of Eq. 1 because the time dependence on activation energy is exponential. If the numerical values calculated are within the order of magnitude of measured values, the exercise is regarded as successful because of these high exponential sensitivities. This is one reason why the SCC data are also presented as a distribution of values rather than a single value (Staehle, 2001).

For slip dissolution or oxidation models, the activation energy for oxidation (e.g., nickel) is closer to those for SCC initiation and ordering. For example, the activation energy for nickel oxidation requires 154 kJ/mol (250–500 ˚C) (Unutulmazsoy et al., 2017); 184 kJ/mol (816–1371 ˚C) (Progen and Lewis, 1964); and 221 kJ/mol (900–1300 ˚C) (Rosa, 1982). These values are comparable with activation energy for ordering. The activation energy for chromium oxide is higher (Kofstad, 1972). Therefore, it is expected that the initiation times for ordering and nickel oxidation (i.e., slip dissolution or oxidation models) could be comparable. As noted above, this level of activation energy also will affect the initiation time very sensitively within the uncertainty range. It is generally understood that intergranular carbides favor SCC. Park et al. (1994) claimed that the activation energy for carbide formation in Alloy 600 is 140 kJ/mol for a water -quenched specimen and lowers further with plastic deformation. Even with this level of activation energy, it will take a long time to nucleate carbides at lower temperatures. Higher

activation energy for the topographically close -packed phase (TCP) and carbide formations is also reported to be greater than 260 kJ/mol for nickel-l-based alloys (Bechtel SAIC Company, LLC, 2004). -Subsequent tests show that this activation energy is related to the ordering process (Kim et al., 2000) and that the form of intergranular carbides may assist ordering in Alloy 690 (Mouginot et al., 2017). Increased carbon concentration actually slows down ordering (Kim et al., 2000).

With regard to the activation energies stated above, the energies are mainly supplied by thermal means (i.e., temperature rise). Ahn (2018) presents the magnitude of alternative energies such as stress in the absence of significant thermal energy (i.e., at low temperature). The exercise results state that about 10,000 MPa stress is needed to activate the above-mentioned kinetics of ordering or SCC without thermal energy. Therefore, it is very unlikely that the reactions above would happen at low temperatures in a short timeframe.

The activation energy for SCC propagation of Alloy 600 is generally about 60 kJ/mole less than the activation energy for SCC initiation. As analyzed above on stress contribution to the activation energy, the bulk stress (either from ordering or residual stress) can contribute to crack formation heterogeneously in thin oxide film or grain boundaries, effectively increasing the local stress. However, the energy input associated with stress for oxidation or ordering is insignificant compared to the thermal energy (Ahn, 2018). High temperature is still needed even in the presence of any stress for SCC to occur. Another more likely contributor to the activation energy is from any increase of anodic potential from crevice (localized corrosion principle) or ordering (Furuya and Motoo, 1976). Cracks were observed in the crevice of the steam generator of a nuclear reactor.

The energy associated with potential is written by:

$$\text{Energy} = n \times \varepsilon \times F \qquad \text{(Eq. 2)}$$

where:

n is charge transfer valence,
ε is electrode potential, and
F is Faraday constant (Capacitant).

This Eq. can also be written by Volt (V) times Coulomb. Using an example for nickel--based alloys, 0.25 V and n = 2 (SNL, 2007), the energy is approximately 50 kJ/mole to assist crack nucleation. As used by Shukla et al (2006), the polarization by 0.7 V (with respect to repassivation potential) will result in 140 kJ/mole, closer to the thermal activation 140 kJ/mole, closer to the thermal activation energy. This level of energy, 0.25 V, is also similar to lower activation energy for SCC propagation compared to the SCC initiation. Once the crack propagates, the electrode may keep lower potential. This electrochemical potential effect on SCC is also consistent with the NRC's evaluation (Stahle (NRC), 2006; Staehle, 2001). More recent studies of SCC propagation by Lee and Macdonald (2018) adopt this approach too at lower temperature. It appears that stress/stress intensification determines electrochemical conditions (e.g., geometry) rather than supplying direct energy. This could be another reason why the crack growth rate is generally independent of stress/stress intensification factor.

3.5 Stress, Strain Rate, and Plastic Deformation

Special Metals presents a database on time--temperature--stress for rupture. It is generally known as the Larson Miller correlation. The database provides a temperature–stress relation above 510 ˚C for up to 11.4 years. This correlation is extrapolated to 315 ˚C by a simple Arrhenius correlation. This extrapolation provides approximately 160 MPa from an initial 510 MPa; approximately 110 MPa from an initial 350 MPa, after 11.4 years. Therefore, the residual stress is likely to be present after reactor operations of longer than 10 years. There may be some stress generation during the ordering process from lattice contraction. Young et al. (2013) measured the compressive stress development up to greater than 200 MPa in 1.14 years and suggested that heterogeneous planar slip may occur. However, so far there was no crack development observed in air from the ordering -related process (e.g., in air) without applied stress. Any heterogeneous stress distribution from the compressive stress (Young et al., 2013) developed could have led to cracks during the aging practices in air for ordering studies without involving water, but no cracks were observed. In water, yield stress is known to initiate/propagate SCC cracks, and the yield stress decreases at higher temperatures over a longer time, as discussed in relation to stress relaxation/creep (i.e., the Larson Miller correlation) (Special Metals). Potential ordering increases hardness, which in turn increases yield stress, possibly resulting in being less prone to SCC.

The effects of stress on SCC have been studied. In general, the SCC initiation time is inversely proportional to the "n^{th}" (where n is an integer greater than 1) power of stress (Scott, 2018). This relation is derived here by nucleation kinetics for ordering (or broadly oxidation too) in terms of stress (or stress intensification) as a driving force for nucleation (Ahn, 2018). Actual data by Vaillant and Le Hong (1997) report that the SCC initiation time is more independent of the plastic strain (above 5 %) and considered infinite at no plastic strain. In stress–SCC initiation times measured, similarly, the log initiation time is correlated to linear stress, but the dependence on stress is weak (Casagne et al., 1992; Special Metals). This is understandable because the "nth" power dependence is a very steep slope.

The strain rate effects were discussed above in Section 3.1. There are optimum conditions of strain rate under which SCC would occur (Jones, 1992; Ugiansky and Payer, 1979),i.e., harmonization. These optimum ranges are harmonics of repassivation rate, mechanical failure, dislocation (or other defects) dynamics, or other intrinsic solid properties (e.g., internal friction, Anderson, et al., 2017). Based on these understandings, in the SCC initiation state, the static loading cannot be simulated by dynamic loading (slow strain -rate tests) as a time -acceleration method. As mentioned in Section 3.1, under static stress, the closest initial condition for crack initiation/propagation is yield stress. It is likely that slow strain -rate tests are only used as SCC screening tests. More broadly, each temperature also has a unique energy level, which can be converted to its own frequency. Increasing temperature in a range provides a more harmonic frequency. This is the reason why SCC occurs in a certain range of temperature over a given time period.

In the ordering transformation, plastic strain is known to slow down the ordering process because the plastic strain makes the disorder state more severe. Young et al. (2013) reported that cold worked material tends to show higher apparent activation energy to approximately 200 kJ/mol from furnace cooled material, and approximately 155 kJ/mol for high chromium model binary alloys. Therefore, it is expected that plastic strain will delay the ordering process.

3.6 Electrode Potential Drop, Rate-Limiting Step, and Data Uncertainties (Statistics)

Past reactor SCC studies have emphasized the significance of electrochemical potential (Stahle (NRC), 2006, Staehle, 2001), as mentioned above in Section 3.4. Generally, ordered anodic oxide forms in many metals, such as aluminum and titanium. Further, the reverse of order-to-disorder phase with anodic potential was reported in metals (Furuya and Motoo, 1976). In this regard, the ordering process may induce electrode potential change. In reactor operations, SCC initiates in the crevice area. In the crevice, the electrode potential is polarized because of the occluded water chemistry that is different from the outside water. In an actual SCC (slow strain rate) test of nickel-based alloys at near to 100 ˚C, SCC was initiated only under electrochemical polarization, ~ 0.7 Volt (from repassivation potential, Shukla et al., 2006). A slow strain-rate test of Alloy 600 showed SCC in the absence of oxygen at 360 ˚C (Kim et al., 2015), implying the electrode potential change, while crystalline ordering was also observed. Lastly, it is well known and practiced that hydrogen dissolved in reactor water suppresses the SCC initiation. Hydrogen is considered to alter the electrode potential. In the data presented above in Section 2, Table, the inclusion of hydrogen in water was mentioned whenever used. From these studies, it can be deduced that (1) the ordering process alters electrode potential, or, alternately, (2) the oxidation alters electrode potential. Both oxidation and ordering may promote the SCC initiation. As the ordering or oxidation times seem to be closer, both seem to be possible as of now. Additionally, TCP and carbide formation may assist/come together with ordering or oxidation over the long term at a lower temperature, as mentioned above.

Crack initiation rates involve several steps. These steps are related either in series or in parallel. In the series relation, the slower rate controls the overall observed rate. In the parallel relation, the faster rate controls the overall observed rate. In a simple case of SCC initiation, one can consider steps of ordering, oxidation, crack formation (e.g., film rupture), and crack propagation. The ordering or oxidation could occur in series (in both ways), alternately, or simultaneously, depending on water chemistry and temperature. As mentioned earlier in this paper, the activation energies are similar for both cases, potentially leading to similar SCC initiation times.

Finally, the data uncertainties are large because of the exponential dependence on the kinetics involved. The exponent activation energies are affected sensitively by alloy chemistry and crystalline defects (e.g., point defects), secondary phase formation (e.g., TCP/carbide), or fabrication process (e.g., temperature, time, and stress). This is the reason that statistics are also used in the data interpretation (Staehle, 2001).

3.7 Low -Temperature Stress Corrosion Cracking

For low temperatures, SCC of Alloy 600 below 100 ˚C can be estimated by extrapolating the nucleation kinetics obtained at higher temperatures. The estimates can be very long times (Ahn, 2018; Stephen et al., 2018; Young et al., 2013). There is low activation energy measured at lower temperatures of 25–300 ˚C in sulfuric acid, with 200 ppb oxygen for sensitized Alloy 600 (Andresen, 1993). The activation is very low (e.g., 20 kJ/mol), and there was a maximum crack propagation rate at around 180 ˚C. This peak is normally associated with maximum oxygen dissolved, indicating that electrochemistry is involved other than thermal effects. Of course, the SCC mechanism is different from the reactor case, especially under more oxidizing conditions. It is also noted that sensitization occurred with acceleration at higher

temperatures in just a short time. It is possible that this sensitization may occur at lower temperatures for a very long time.

3.8 Stainless Steel

For stainless steel, it is rare to find the SCC initiation time at above 300 ˚C. Recent studies on SCC propagation of cold-worked 316 and 316L stainless steel showed a few hundred to 2,000 hours (less than 0.23 year) before crack propagation at 325 ˚C and 288 ˚C, respectively, in water containing chloride, oxygen, and hydrogen, and their combinations (Du et al., 2016). Aoki et al. (2018) tested 304L and 316L stainless steel at 288 ˚C for 14,000 hours (1.6 years) under a creviced bent beam. No SCC initiation was observed except in one sample of the 316L steel.

However, substantial data on *failure* times exist at temperatures below 100 ˚C in chloride--induced SCC of 304 stainless steel in water with air. In these cases of the applied static stress (approximately 100–500 MPa), the times are less than 1 month (0.08 year) (Xie and Zhang, 2015; Nakayama and Sakakibara, 2013; Mayuzumi et al., 2008). The differential scanning calorimetry data shows 234 kJ/mol activation energy for 316L stainless steel needed for lattice-order phase transformation (Kim and Kang, 2016). This range of activation energy is equivalent to stress (in terms of energy) far more than the stress used in these SCC tests. The details on the stress required at lower temperature was presented along with this paper (Ahn, 2018). This means that the lower temperature SCC mechanisms for stainless steel are different from potential SCC mechanisms at higher temperatures. For example, as introduced above Lee and Macdonald (2018) and Shukla et al (2006) presented the electrochemical process at lower temperatures. He et al (2014) presented chloride-induced SCC of U bend specimen of stainless steel including no sensitization under relative humidity of 44 % at 45˚C. Both pitting and subsequent SCC occurred. Earlier work and review by Wang et al.(1995) and Pickering (1986) showed that at the bottom of pit crack formed with solid corrosion product in austenitic stainless steel in chloride solution. He added a local electrode potential inside was ~ 0.5 Volt (~ 100 kJ/mol) as aforementioned, suggesting a significant contribution to crack nucleation. Finally, it is noted that the crack initiation time is exponentially related to the potential (Wada et al., 2013; Nakayama and Skakibara, 2013). Due to this sensitivity, below a threshold potential, SCC did occur in the laboratory test time

3.9 Long-Term Threshold Value for Stress-Corrosion Cracking Initiation

There is literature stating that SCC initiation time is inversely proportional to the "n^{th}" power of stress. The reported "n" values are about 2–6. There has been no mechanistic explanation for why such relation exists. Nucleation mechanism is the first potential explanation for the stress (equivalent to driving force, energy, explained below with G_V) dependence shown in Eq. 1.
In assessing long--term initiation of SCC, another remaining question is whether the laboratory measured threshold values (e.g., temperature, stress, stress intensification factor, electrochemical potential for a cracking rate--limiting precursory pitting) are valid over a long timeframe. One way to check is to scale down the variable, as shown above in an example on stress effect. The variable is approximated in inverse "nth" power and exponential, both in incubation time, as shown in Eq. 1. The initial nuclei population time in more detail (Ahn, 2018) is given in Eq. 1.

$$\Delta G^* \times \exp(\Delta G^*/[RT]) \times \exp(E_m/[RT]) \qquad \text{(Eq. 1)}$$

where:

ΔG^* is activation energy for nuclei population and
E_m is diffusivity for atomic movement for transformation.

ΔG^* is, in turn, the "n^{th}" power for Y_m^3/G_v^2, where Y_m interface energy and G_V driving force. The driving force can be thermal energy (i.e., temperature, stress, and other) (Ahn, 2018, 1996). The apparent activation energy is the sum of the values of ΔG^* and E_m, and the apparent values are measured during SCC kinetic studies at various temperatures.

This exponential in Eq. 1 is mainly from determining substantial initial population of stable nuclei. Under these conditions, the initiation times will increase rapidly as parameter values decrease below threshold values. For example, the driving force, G_v, is proportional to the square of stress intensification, K. The activation energy, ΔG^*, is, in turn, inversely proportional to the 4^{th} power of K. Therefore, if the K value is lowered below the threshold value by a factor of 2, the incubation time will be very long, with 190 kJ/mole activation energy. This does not include the time increase from the pre-exponential term in Eq. 1. Nuclear and other industries experienced SCC of stainless steel with very long incubation times of 10–20 years (Chu et al., 2014). Until the K value becomes bigger, cracks may not initiate at lower temperatures. At low temperatures, such situations may occur with pit growth with chlorides. It is likely that the most significant and sensitive contributor in cracking time is crack (such as slip or void) formation energy, especially when the stress or stress intensification factor is low (e.g., stress below yield stress). These example exercises of threshold stress values can be extended to other involved variables, such as pitting potential, pit depth, or creep rate, as rate--limiting precursory steps for crack formation over a long timeframe.

3.10 Potential Applications

The studies presented here would be considered for long-term issues in nuclear energy systems. This approach could be more efficiently considered with inspections (if possible) and a probabilistic approach (Ahn, 2013; Staehle, 2001). Alloy 600 was chosen because it has more controlled data. The analysis made here would potentially apply to other nuclear component materials, including stainless steel, carbon steel, and zirconium alloys.

4. Summary

(1) This paper summarized initiation times of SCC in Alloy 600 (and related alloys) in simulated or real reactor environments near 300 ˚C.

(2) An analysis was conducted and summarized. For this purpose, important traditional SCC mechanisms were also summarized.

(3) This paper referenced a crystalline ordering process from Ahn (2018). The initiation times for the ordering process were somewhat comparable to the traditional SCC initiation times.

(4) Traditional mechanisms, such as slip dissolution or oxidation models (along with carbide/TCP), were proposed to occur nearly simultaneously with the crystalline ordering mechanism. To support this proposal, other observations were also evaluated, including

activation energy, stress/strain rate/plastic deformation, electrode potential drop, rate- -limiting step, data uncertainties, and long--term threshold values.

(5) The review and analysis made in nickel-based alloys is extended to stainless steels, which are also widely used in nuclear industry.

(6) Based on this review and analysis at higher temperatures, this paper also addressed the understanding of SCC at lower temperatures. Lower temperature SCC of nickel-based alloys and stainless steels has different mechanisms compared to SCC at higher temperatures.

(7) Finally, the paper described how the current work would be applied in nuclear industry.

5. Acknowledgments

The NRC Office of Nuclear Material Safety and Safeguards, Division of Spent Fuel Management, has approved this paper. The paper was NRC peer reviewed by Dr. Yi-Ming Pan of Southwest Research Institute®, San Antonio, TX, and Dr. Appajosula Rao of the NRC.

6. References

(NRC Agencywide Documents Access and Management System (ADAMS) documents: in *Google*, type MLxxxxxxxxx, or visit the NRC ADAMS Web Site, http://www.nrc.gov/ADAMS)

Ahn, 2018 T. Ahn
Nucleation kinetics of crystalline ordering in Alloy 600 at elevated temperature
NRC ADAMS Accession No. ML17129A396 (2018)

Ahn, 2013 T. Ahn
An approach to model abstraction of stress corrosion cracking damage in management of spent nuclear fuel and high-level waste
Proceedings of the ASME 2013 Pressure Vessels & Piping Division Conference, PVP2013, Paris, France, July 14–18, 2013, Paper PVP2013-97139 (2013)

Ahn, 1996 T. Ahn,
Dry oxidation and fracture of LWR spent fuels
NUREG-1565, U.S. Nuclear Regulatory Commission, Washington, DC, NRC ADAMS Accession No. ML040150720 (1996)

P. Anderson, J.P. Hirth and J. Lothe, Theory of Dislocations, 3rd Edition, Cambridge University Press, NY, NY, 2017

Andresen and Chou, 2018 P. Andresen, P. Chou
Crack initiation of Alloy 600 in PWR water
Proceedings of the 18th International Conference on Environmental Degradation of Materials in Nuclear Power Systems—Water Reactors, August 13–17, 2017, Portland,

OR, pp. 121–135 (2018)

Andresen, 1993 P.L. Andresen
Effects of temperature on crack growth rate in sensitized type 304 stainless steel and Alloy 600
Corrosion, 49 (9) (1993) 714–725, Houston, TX: NACE International

Andresen and Ford, 1985 P.L. Andresen, F.P. Ford
Modeling and life prediction of stress corrosion cracking in sensitized stainless steel in high-temperature water
Predictive Capabilities in Environmentally Assisted Cracking, Presented at the Winter Annual Meeting of the American Society of Mechanical Engineers, Miami Beach, FL, November 17–22, R. Rungta, ed., PVP-Vol. 99, pages 17–38, New York, NY: American Society of Mechanical Engineers (1985)

Angeliu et al., 1995 T.M. Angeliu, D.J. Paraventi, G.S. Was
Creep and intergranular cracking behavior of nickel-chromium-iron-carbon alloys in 360 °C Water
Corrosion, 51, No. 11, pp. 837–848 (1995)

Aoki et al., 2018 S. Aoki, K. Kondo, Y. Kaji, M. Yamamoto
Effect of long-term thermal aging on SCC initiation susceptibility in low carbon austenitic stainless steels
Proceedings of the 18th International Conference on Environmental Degradation of Materials in Nuclear Power Systems—Water Reactors, August 13–17, 2017, Portland, OR, pp. 663–672 (2018)

Arioka, 2015 K. Arioka
Changes in bonding strength at grain boundaries before long-term SCC initiation
Corrosion, 71, No. 4, pp. 403–419 (2015)

Bechtel SAIC Company, LLC, 2004
Aging and phase stability of waste package outer barrier
ANL-EBS-MD-000002, Revision 02 (2004)

Capell and Was, 2007 B.M. Capell, G.S. Was
Selective internal oxidation as a mechanism for intergranular stress corrosion Cracking of Ni-Cr-Fe alloys
Metall. Mater. Trans. A, 38A, pp.1244–259 (2007)

Casagne et al., 1992 T.B. Casagne, P. Combrade, M.A. Foucault, A. Gelpi
The influence of mechanical environmental parameters on the crack growth behavior of Alloy 600 in PWR primary water
Twelfth Scandinavian Corrosion Congress and Eurocorr ‘92, pages 55–67, Espoo, Finland, May (1992)

Chu et al., 2014 S. Chu, J. Gorman, K. Fuhr, J. Brousard
Literature review of environmental conditions and chloride-induced degradation relevant to stainless steel canisters in dry cask storage systems

3002002528, Electric Power Research Institute (2014)

Du et al., 2016 D. Du, K. Chen, H. Lu, L. Zhang, X. Shi, X. Xu, P. Andresen
Effects of chloride and oxygen on stress corrosion cracking of cold worked 316/316L austenitic stainless steel in high temperature water
Corr. Sci. 110, pp. 134–142 (2016)

Dunn et al., 2004 D.S. Dunn, D. Daruwalla, Y.M. Pan
Effect of fabrication processes on material stability—characterization and corrosion
Center for Nuclear Waste Regulatory Analyses (CNWRA), CNWRA 2004-01, San Antonio, TX, NRC ADAMS Accession No. ML040480526 (2004)

Economy et al., 1987 G. Economy, R.J. Jacko, F.W. Pement
IGSCC behavior of Alloy 600 steam generator tubing in water or steam tests above 360 °C
Corrosion, 43, No. 12, pp. 727–734 (1987)

Ford and Andresen, 1988 F.P. Ford, P.L. Andresen
Development and use of a predictive model of crack propagation in 304/316L, A533B/A508 and Inconel 600/182 Alloys in 288 °C water
Proceedings of Environmental Degradation of Materials in Nuclear Power Systems—Water Reactors, Proceedings of the Third International Symposium, Traverse City, MI, August 30–September 3, 1987. G.J. Theus and J.R. Weeks, eds.
pages 789–800, Warrendale, PA: Metallurgical Society (1988)

Furuya and Motoo, 1976 N. Furuya, S. Motoo
The electrochemical behavior of ad-atoms and their effect on hydrogen evolution: part 1. order-disorder rearrangement of copper ad-atoms on platinum
J. of Electroanalytical Chemistry and Interfacial Electrochemistry, 72, Issue 2, pp. 165–175 (1976)

Garud and McIlre, 1986 Y.S. Garud, R. McIlree
Intergranular stress corrosion cracking damage model: an approach and its development for Alloy 600 in high-purity water
Corrosion, 42, No. 2, pp. 99–105 (1986)

Grimmel and Cullen, 2005 B. Grimmel, W.H. Cullen
U.S. plant experience with Alloy 600 cracking and boric acid corrosion of light-water reactor pressure vessel materials
NUREG-1823, U.S. Nuclear Regulatory Commission, Washington, DC (2005)

He et al., 2014 X. He, R. Pabalan, T. Mintz, G. Oberson, D. Dunn, T.Ahn
Stress corrosion cracking of UNS S30400 stainless steel exposed to atmospheric Ammonium nitrate and sodium chloride mixtures, CORROSION 2014, Paper No. 3885, NACE (2014)

Jackson et al., 2018 J.H. Jackson, M. Wright, D. Paraventi
edited, TMS, **Proceedings of the 18th International Conference on Environmental**

Degradation of Materials in Nuclear Power Systems—Water Reactors, Vol. 1 (2018)

Jones, 1992 R.H. Jones
editor, **Stress-corrosion cracking**
ASM International, Materials Park, OH (1992)

Kim and Kang, 2016 S.S. Kim, S.H. Kang
Effect of short range ordering reaction and ordering treatment on microstructure in 316L stainless steel
Korea Atomic Energy Research Institute (2016)

Kim et al., 2015 Y.S. Kim, Y.W. Maeng, S.S. Kim
Effect of short-range ordering on stress corrosion cracking susceptibility of Alloy 600 studied by electron and neutron diffraction
Acta Mater, 83, pp. 507–515 (2015)

Kim et al., 2000 S.S. Kim, I.H. Kuk, J.S. Kim
Order-disorder reaction in Alloy 600
Mater. Sci. Eng.A, A279, pp.142–148 (2000)

Kofstad, 1972 P. Kofstad
Nonstoichiometry, diffusion, and electrical conductivity in binary metal oxides
Wiley-Interscience, New York (1972)

Lee and Macdonald, 2018 S.-K. Lee, D.D. Macdonald
Theoretical aspects of stress corrosion cracking of Alloy 22
J. Nucl. Mater. 503, pp. 124–139 (2018)

Léonard, 2010 F. Léonard
Study of stress corrosion cracking of Alloy 600 in high temperature high pressure water
Doctor of Philosophy Thesis, University of Manchester, Manchester, United Kingdom (2010)

Mayuzumi et al., 2008 M. Mayuzumi, J. Tani, T. Arai
Chloride induced stress corrosion cracking of candidate canister materials for dry storage of spent fuel
Nucl. Eng. Des. 238, pp. 1227–1232 (2008)

Moss et al., 2018 T.E. Moss, T.E., C. M. Brown, G.A. Young
The effect of hardening via long range order on the SCC and LTCP susceptibility of a nickel-30 chromium binary alloy
Proceedings of the 18th International Conference on Environmental Degradation of Materials in Nuclear Power Systems—Water Reactors, Vol. 1, TMS, edited by J.H. Jackson, M. Wright and D. Paraventi (2018)

Mouginot et al., 2017 R. Mouginot, T. Sarikka, M. Heikkilä, M. Ivanchenko, U. Ehrnstén, Y.S. Kim, S.S. Kim, H. Hänninen
Thermal ageing and short-range ordering of Alloy 690 between 350 and 550 °C

J. Nucl. Mater. 485, pp. 56–66 (2017)

Nakayama and Sakakibara, 2013 G. Nakayama, Y. Sakakibara
Prediction model for atmospheric stress corrosion cracking of SS
ECS Transaction, 50 (31), pp. 303–311 (2013)

Park et al., 1994 J.M. Park, W.S. Ryu, Y.H. Kang
DSC Study on Carbide precipitations reaction in Inconel 600
J. Nucl. Mater. 209, pp. 221–225 (1994)

Pickering, 1986 H. W. Pickering
On the roles of corrosion products in local cell processes
Whiney Award, The Pennsylvania State University, Lecture Paper, Office of Naval Research Annual Report, 1986

Progen and Lewis, 1964 D.J. Progen, B.W. Lewis
A study of oxidation kinetics of nickel metal in flowing air and oxygen-nitrogen mixture
NASA Technical Note, NASA D-2224, Langley Research Center, NASA, Langley Station, Hampton, VA (1964)

Richey and Morton, 2005 E. Richey, D. Morton.
Stress corrosion cracking initiation of Ni-based alloys in high temperature water
LM-05K031, March 21, 2005, CORROSION/2005 Conference, Houston, TX, April 3–7 (2005)

Rosa, 1982 C.J. Rosa
The high temperature oxidation of nickel
Corr. Sci. 22, pp. 1081–1088 (1982)

Scott, 2018 P.M. Scott
An overview of materials degradation by stress corrosion in PWRs
(2018)

Scott, 2013 P.M. Scott
PWSCC of nickel base alloys and mitigation in PWRs
Presented at the INL Seminar on SCC in LWRs, Idaho Falls, ID, March 19–20 (2013)

Scott and Le Calvar, 1993 P. Scott, M. Le Calvar
Some possible mechanisms of intergranular stress corrosion cracking of Alloy 600 in PWR primary water
In Fourteenth international Conference on Environmental Degradation of Materials in Nuclear Power Systems—Water Reactors, pp. 657–667, San Diego, CA, TMA, August (1993)

Shen et al., 2018 Z. Shen, K. Arioka, S. Lozano-Perez
A mechanistic study of SCC in Alloy 600 through high-resolution characterization
Corr. Sci. 132, pp. 244–259 (2018)

Shukla et al., 2006 P.K. Shukla, D.S. Dunn, K.-T. Chiang, O. Pensado
Stress corrosion cracking model for Alloy 22 in the potential Yucca Mountain Repository environment
Proceedings of the CORROSION/2006 Conference. Paper No. 06502. Houston, TX: NACE International (2006)

SNL (Sandia National Laboratories), 2007
General corrosion and localized corrosion of waste package outer barrier
ANL-EBS-MD-000003, Revision 03 (2007)

Special Metals
INCONEL® alloy 600
www.specialmetals.com

Stahle, 2006 W. Stahle
Assessment of internal oxidation (IO) as a mechanism for submodes of stress corrosion cracking (SCC) that occur on the secondary side of steam generator
NUREG/CR-6827, U.S. Nuclear Regulatory Commission, Washington, DC, RWS 154 (2006)

Staehle, 2001 R.W. Staehle
Bases for predicting the earliest failures due to stress corrosion cracking
In: Chemistry and Electrochemistry of Corrosion and Stress Corrosion Cracking: A Symposium Honoring the Contribution of R.W. Staehle, A Publication of the Minerals, Metals, & Materials Society, Warrendale, PA (2001)

Stephen et al., 2018 B. Stephen, B., D. Jacob, F. Delabrouille, L. Legras
A kinetic study of order-disorder transition in Ni-Cr based alloys
Proceedings of the 18th International Conference on Environmental Degradation of Materials in Nuclear Power Systems-Water Reactors, Vol. 1, TMS, edited by J.H. Jackson, M. Wright and D. Paraventi (2018)

Ugiansky and Payer, 1979 G.M. Ugiansky, J.H. Payer
editor, **Stress-corrosion cracking**
ASM International, Materials Park, OH (1979)

Unutulmazsoy et al., 2017 Y. Unutulmazsoy, R. Merkle, D. Fischer, J. Mannhart, J. Maier
The oxidation kinetics of thin nickel films between 250 and 500 °C
Phys. Chem. Chem. Phys., 19, pp. 9045–9052 (2017)

Vaillant and Le Hong, 1997 F. Vaillant, S. Le Hong
Evaluation de la vitesse de propagation en milieu primaere de matériaux traverses de cuvee n alliage 600 et de métaux deposes en alliage 182
Technical Report HT-44/96/024/A, EDF R&D (1997)

Y. Wada, A. Watanabe, K. Shida, M. Tachibana, M. A. Aizawa and M. Fuse, **Intergranular stress corrosion crackign initiation model of austenitic stainless steels used in BWRs for optimized water chemistry control,** J. Nuclear Science and Technology,

50:5, pp. 546 – 555 (2013)

M. Wang, H.W. Pickering and Y. Xu, **Potential Distribution, Shape Evolution and Modeling,** J. Electrochemical Society, Vol. 142, pp. 2986 – 2995 (1995)

Xie and Zhang, 2015 Y. Xie, J. Zhang
Chloride-Induced Stress Corrosion Cracking of Used Nuclear Fuel Welded Stainless Steel Canisters: A Review
J. Nucl. Mater. 4I66, pp. 85–93 (2015)

Yi et al., 2013 Y. Yi, G. Was, J. Cookson, J. Fish, S. Attanasio, H. Krasodomski, W. Wilkening
Creep of Nickel Base Alloys in High Temperature Water
Proceedings of the 9th International Conference on Environmental Degradation of Materials in Nuclear Power Systems—Water Reactors, TMS, edited by S. Bruemmer, P. Ford and G. Was (2013)

Yonezawa, 2013 T. Yonezawa
in Y.S. Kim, S.S. Kim, D.W. Kim, **Intergranular stress corrosion cracking (IGSCC) of Alloy 600 with cooling rate**, in Proceedings of 16th International Symposium on Environmental Degradation of Materials in Nuclear Power Systems—Water Reactors, Asheville, NC, TMS, Warrendale, PA (2013)

Yoo et al., 2018 S.C. Yoo, K.J. Choi, S. Kim, J.-S. Kim, B.H. Choi, Y.-J. Kim, J.-S. Kim, J.H. Kim
PWSCC initiation of Alloy 600: effect of long-term thermal aging and triaxial stress
Proceedings of the 18th International Conference on Environmental Degradation of Materials in Nuclear Power Systems—Water Reactors, Vol. 1, TMS, edited by J.H. Jackson, M. Wright, and D. Paraventi (2018)

Young et al., 2013 G.A. Young, J.D. Tucker, D.R. Eno
The kinetics of long range ordering in Ni-Cr and Ni-Cr-Fe Alloys
Proceedings of the 16th International Conference on Environmental Degradation of Materials in Nuclear Power Systems—Water Reactors 2013, Ashville, NC, August 11–15, 2013, NACE International, pp. 13–34 (2013)

Zhai et al., 2015 Z. Zhai, M.J. Olszta, M.B. Toloczko, S.M. Bruemmer
Summary of stress corrosion crack initiation measurements and analyses on Alloy 600 and Alloy 690
M2LW-15OR0402034 (2015)